

Mechanics of Advanced Composite Structures

Journal homepage: https://macs.semnan.ac.ir/

ISSN:2423-7043



Research Article

Comparative Investigation of Deflection in a Bi-directional Curved Functionally Graded Porous Beam Using Unified Shear Deformation Theory

Gangi Reddy Gari Chandra Mohana Reddy^{a*}, B<mark>ridjesh Pappula^b, Ch. Ravi Kirana, S. Nagarajua</mark>

^a Department of Mechanical Engineering, MLR Institute of Technology, Hyderabad,500043, India

^b Department of Chemical <mark>&Materials Engin</mark>eering, College of Science, Engineering and Technology, University of South Africa (UNISA), c/o Christiaan de Wet; Pioneer Avenue, Florida Campus 1710, Johannesburg, South Africa.

ARTICLE INFO

ABSTRACT

Article history:

Received: 2023-03-22 Revised: 2023-05-12 Accepted: 2023-10-19

Keywords:

Curved porous beam; Bending characteristics; Unified shear deformation theory; Porosity. The present study investigates the bending characteristics of a two-dimensional functionally graded curved porous beam using unified shear deformation theory (USDT), incorporating shear functions and a modified power law. This approach integrates potential energy, the neutral surface concept, and equilibrium equations to enhance accuracy. Various boundary conditions, such as simply supported (SS), clamped-supported (CS), clamped-clamped (CC), and clamped-free (CF), are employed in the analysis. A metal-ceramic functionally graded beam with both even and uneven porosity is modelled. The symmetrical material gradation ensures that the physical neutral surface aligns with the geometrical neutral surface, which is considered in the formulation. A displacement-based formulation and energy principles are adopted, providing a more comprehensive and precise analysis of the beams. This method accounts for higher-order shear deformation effects, eliminates the need for shear correction factors, and effectively manages the continuous variation of material properties in FGMs. Consequently, it leads to improved predictions of structural behavior, making USDT particularly valuable for advanced material applications. The Hamilton method is employed to derive equilibrium equations for the beams, which are subsequently solved using the Kuhn-Tucker conditions.

© 2024 The Author(s). Mechanics of Advanced Composite Structures published by Semnan University Press. This is an open access article under the CC-BY 4.0 license. (https://creativecommons.org/licenses/by/4.0/)

1. Introduction

Functionally Graded Materials (FGM) offer numerous benefits like enhanced stress distribution, high temperature tolerance, and strength, making them useful in various technical fields like aerospace, automotive, electrical, construction, and biomedical.

Higher-order theory was used to examine the bending behavior of Functionally Graded (FG) curved Al/Al_2O_3 beams in elevation, considering shear deformation and thickness stretching effects, and examining sandwich beams with

symmetric and asymmetric cores [1]. Lezgy-Nazargah [2] adapted a global-local shear deformation theory for the behavior of Al/Al₂O₃ thin and thick layered curved beams, considering depth and a locally refined shear stress function. Beg et al. [3] introduced a layerwise approach for analyzing static, free, and forced vibrations of circular Al/Al₂O₃curved beams with significant curvature, using the Hamiltonian technique for consistent dynamics and stress results. Sayyad and Avhad [4] analyzed the free vibration of curved sandwich beams in elevation using a fifth-order curved

E-mail address: cmreddy115@gmail.com

^{*} Corresponding author.

beam theory, considering transverse shear and normal strains, and solving equations of motion using Navier's technique. Hadji et al. [5] examined the flexure and natural oscillation of Porous Functionally Graded Beams (PFG) supported by elastic foundations, focusing on their varying material features and foundation medium. Avcar et al. [6] explored the natural frequencies of P/IP-FGSBs, consisting of a porous core made of FGM with aluminum. alumina, and homogenous isotropic metal, and ceramic face sheets supported by elastic foundations. Sayyad et al. [7] examined the static deformation and free vibration of porous circular beams made of aluminum and alumina, considering both even and uneven porosities. The Navier-type closed-form solutions were derived from the higher-order hyperbolic circular beam theory to address transverse shear deformation and rotating inertia. Chami et al. [8] studied FGMs to enhance sandwich beam endurance and examined the impact of porosity on the fundamental natural frequencies of FG sandwich beams using advanced beam theory. Pham et al. [9] examined the hydro-thermal vibration of curved BDFGP beams supported by two-layer elastic foundations. Using GFEM, they analyzed the dynamic behavior of Winkler springs and shear springs, creating an enriched mathematical space. Ahmadi et al. [10] investigated the natural oscillation of a 2D-FG curved nano beam, functionally graded in two directions, using Hamilton's principle and firstorder shear deformation theory. The nonlocal elasticity hypothesis of Eringen accounts for the small-scale effect. Belarbi et al. [11] introduced an improved shear deformation beam theory for analyzing the bending characteristics of functionally graded sandwich curved beams, providing a parabolic variation in shear stress distribution along the thickness direction and eliminating shear correction components. Karamanli et al. [12] analyzed the flexural, free vibration, and buckling responses of 2D-FG curved beams using various shear deformation theories and a finite element model and compared the results to the literature [12].

Advancements in Shear Deformation Theories (SDTs) have recently allowed for thorough assessments of the mechanical behavior of Functionally Graded Beams (FGB), namely those made of aluminum and alumina, under different loading and boundary conditions. Hebbar et al. [13] used SDTs, namely two- and quasi-three-dimensional theories, to examine the behavior of FGB with aluminum and alumina Simply Supported (SS) beams under various circumstances, including vibration, buckling, and bending. In a situation with an SS-FGB with aluminum and alumina and an evenly

distributed load, Razouki et al. [14] established exact analytical solutions. Third-order shear deformation theory was used to formulate specific analytical formulas, which were then compared to both the conventional analytical formula and the currently available numerical data. Reddy et al. [15] investigated the bending response of 2D FGB using a shear strain shape function, examining the impact of gradient index, porosity volume fraction, and aspect ratios. Bridjesh et al. [16] studied the impact of aspect ratios, boundary conditions, and gradient indexes on the buckling responses of two directional FGB using polynomial forms and boundary conditions like SS, Clamped-clamped (CC), and Clamped-free (CF). The influence of porosity, boundary conditions, and gradient indexes on the buckling responses functionally graded beams using a fifth-order shear deformation theory was investigated by Bridjesh et al. [17], and found that the boundary conditions play a significant role in the analysis of beams. In another study, Reddy et al. [18] examined the vibration behavior of a twodirectional functionally graded taper beam using Higher-order Shear Deformation Theory (HSDT), Lagrange equations, and admissible functions, providing a benchmark for beam theory assessment.

in Advancements beam theory and computational approaches have improved the design and analysis of micro- and nano-electromechanical systems, curved beams, and materials with varying properties in multiple directions. The Timoshenko beam theory was adapted to develop a computational approach for designing and optimizing device components in microand nanoelectromechanical systems by combining modified couple stress theory with an isogeometric analysis framework [19]. Pei et al. [20] discussed Navier's solution for curved beams with SS, but the case was mathematically indeterminate. The Timoshenko theory was used for governing differential equations. Wang et al. [21] introduced an extension of the quadrature element method to study the free vibration of 3D parallel pipes made of multidirectional FGM, providing formulations for continuous variations in material characteristics.

Recent studies have thoroughly investigated static bending, vibration, and buckling characteristics of functionally graded porous microplates and plates using modern plate theories and computational approaches. Using a third-order plate theory, Coskun et al. [22] examined static bending, free vibration, and buckling of FG porous microplates. The analytical solutions were derived through the application of Navier's technique. Kim et al. [23],

in their study, utilized classical and first-order shear deformation plate theories to analyze FG porous micro-plates made by aluminum and alumina buckling, vibration, and bending responses using the Navier solution technique and power-law distribution. Saad and Hadji [24] examined the thermal buckling analysis in porous, thick rectangular plates made of FGM using HSDT, considering material properties like Young's modulus and thermal expansion change in thickness direction. Hadji et al. [25] explored the influence of porosity distribution patterns on free vibration analysis in Functionally Graded Porous Plates (FGPP) under different boundary conditions, considering continuous material properties and porosities based on volume fraction. Madan et al. [26] explored the elastic limit of functionally graded porous rotating disks using a method that models their mechanical characteristics using four porosity models and Galerkin's error minimization theory. Yang et al. [27] presented a numerical investigation of the post-buckling behavior of multi-directional FGPPs with aluminum and alumina, combining NURBS-based IGA with FCM. Thai et al. [28] introduced a computational method for analyzing the bending and free vibration characteristics of Functionally Graded Plates (FGP) in three dimensions, considering heat conditions and using generalized heat transfer equations.

Advanced theoretical and computational methods have been used to analyze the intricate behaviors of porous FG plates, with a focus on examining the plate's free vibration, bending, buckling, and thermal impacts. Chami et al. [29] examined free vibration on a sandwich plate multi-directional porous FGM, using Hamilton's concept and Navier's approach. The plate was examined under two conditions, avoiding surface traction and using shear correction coefficients. Hadji et al. [30] examined the bending and buckling of a multidirectional porous sandwich plate, considering two cases with FG skin and a homogeneous core, using Navier's approach to achieve a solution without shear correction factors. Adopting HSDT, Sidda Reddy et al. [31] developed a static analysis of FGP, demonstrating its accuracy and efficiency in predicting static responses. They developed analytical formulations for free vibration analysis of FGPs using HSDT, incorporating transverse extensibility, virtual work, and Navier's technique. The closed-form formulations of HSDT for analyzing FGP under thermo-mechanical load conditions confirm its exactness and consistency through numerical results [32, 33]. Sidda Reddy et al. [34] explored the flexural response of FGPs with porosities using an HSDT, demonstrating its accuracy and

consistency through numerical results. Sidda Reddy et al. [35] presented a refined first-order shear deformation theory for studying the free vibration behavior of bidirectional functionally graded porous plates, evaluating its accuracy through numerical results and comparing it with other higher-order theories. Sidda Reddy et al. [36] optimized plate design by analyzing buckling in in-plane bidirectional functionally graded porous plates using higher-order theory, Lagrange equations, and Pascal's triangle. Sidda Reddy et al. [37] analyzed the bending of FGPs using a new shear strain shape function, revealing that the type of porosity distribution is crucial for the optimal design of porous FGPs.Sinusoidal beam theory was explored for the static behavior of FG sandwich curved beams, considering transverse normal stress/strain. The beam consists of FG skins and an isotropic core. Material qualities distributed throughout the thickness [38]. In their study, Karamanli and Vo [39] explored the free vibrations of curved zigzag nanobeams using sinusoidal beam theory and doublet mechanics formulation, developing a finite element doublet mechanics model comparing results.

Rezaiee-Pajand and Masoodi [40] conducted an extensive study of functionally graded tapering beam-columns, including second-order effects, coupling-extensional bending, and semirigid connections using a generic stiffness matrix formulation. The suggested technique accurately assesses the stability and buckling behavior of 2D frames, showcasing its efficacy and relevance via comparisons with established solutions.

Rezaiee-Pajand et al. [41] developed a highbeam performance curved element for geometrically nonlinear analysis of planar structures using mixed strain finite rotation. interpolation and The proposed element, incorporating **FSDT** and Green-Lagrange strain, effectively models tapered structures and demonstrates accuracy with fewer elements.

Ghandehari et al. [42] developed a model for a linked nanocomposite double beam system using carbon nanotubes, including temperature-dependent material characteristics and diverse CNT distributions throughout the thickness. Employing first-order shear deformation theory and the GDQ technique, the fundamental frequencies are calculated to examine the influence of structural and thermal components on dynamic behavior.

Mottaghi et al. [43] studied the vibrational behavior of CNT-reinforced curved composite beams using a multiscale FEM approach and evaluated the first natural frequency under various configurations.

A multilayer perceptron neural network, trained on FEM data, predicts the frequency with over 95% accuracy, demonstrating the model's reliability for dynamic analysis of composite structures.

Masoodi et al. [44] examined the heat sensitivity of vibrational features in CNT-reinforced coupled curved beams by using temperature-dependent material properties and first-order shear deformation theory. A meshfree GDQ-based approach is used to calculate frequency responses, demonstrating the effects of curvature, boundary conditions, interfacial stiffness, and CNT dispersion on dynamic behavior.

Ghandehari et al. [45] studied the dynamic response of tapered circular curved beams with honeycomb-shaped cross-sections using FSDT and GDQM, considering smart composite materials and structural parameters. The results show that the CNT honeycomb geometry, content. spring and boundary stiffness have significant effect on natural frequencies, which indicates the improved vibrational performance of smart composites.

Ghandehari and Masoodi [46] investigated the thermal vibration characteristics of linked porous curved beams constructed from diverse materials, including PMMA/SWCNT composites and steel foam, using the First-Order Shear Deformation Theory (FSDT) and the Generalized Differential Quadrature (GDQ) technique. Results indicate that system frequencies are affected by porosity, material markedly distribution, conditions, boundary temperature, with increased porosity and temperature leading to a reduction in vibrational frequencies.

A comprehensive literature review on the proposed research topic has been conducted and presented. Studies on structural analysis in the field of FG curved beam/straight beam /plate subjected to transverse loading are abundant in the literature. In most cases, the material properties of the beam vary continuously in the direction of thickness according to a power law. In a significant number of the reviewed works, geometric nonlinearity and the resulting large displacement are discussed. In certain instances, non-uniform geometry is considered in static and dynamic analysis. There are also works on Euler-Bernoulli beam theory available in the literature. Infrequently, nonlinear analysis is cited. In some instances, non-uniform geometry is also considered.

This study introduces a novel approach by employing the Kuhn-Tucker (KT) condition solution method for bending analysis in FG porous structures, aiming to enhance existing methodologies and uncover the relationship between material classification and porosity distribution, potentially revealing unique phenomena. The research focuses on the flexural characteristics of curved beams with Two-directional Functionally Graded Porous Beam (2DFGPCB) using Unified Shear Deformation Theory (USDT) to develop a comprehensive mathematical model, accounts for deflections and conducts a detailed bending analysis. The innovative methodology will be validated through a comparative analysis with established numerical methods.

2. Mathematical Formulation

According to HSDT, a beam is conceptualized as a slender structural component that exhibits shear and bending properties. The beam is considered to have a curved geometry with spatially varying material properties along its radial and axial directions, as characterized by a bi-directional functional gradation. Warping effects, which involve the twisting of the crosssection, are not considered. Instead, it is assumed that the cross-sections, which were initially flat, remain flat following deformation. The assumption is made that the material properties remain consistent along the entire length of the beam, which allows for easier computations and analytical solutions. The current study used the coordinate system depicted in Fig. 1 for a 2DFGPCB. Both length and thickness dimensions exhibit continuous variation in the material properties. The thickness-dependent variation of ceramic and metallic phases symbolizes the FG curved beam. At z = -h/2, the lower section of the beam is constructed of metal, whereas at z = +h/2, the upper segment is composed of ceramic.

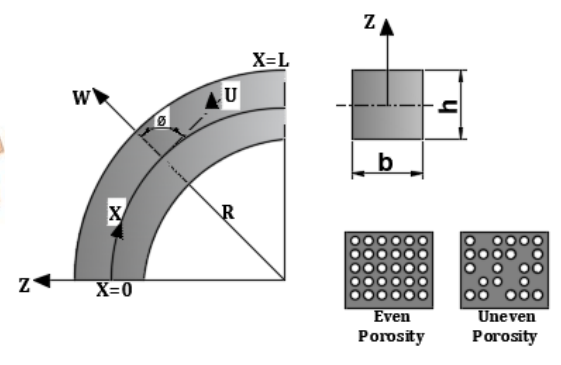


Fig. 1. Beam characterized by functional grading and varying porosity

2.1. Material Homogenization

The fabrication of FGB is influenced by the volumetric composition of the constituent materials. A functional and structural relationship between the thickness and properties of the material is to be anticipated.

The power law distribution in x and z, represented as (Vf_1) , provides an accurate representation of the volume fraction of a single constituent, as illustrated in Eqs. (1) and (2) [12].

$$V_{f1}(x,z) = \left(\frac{z}{h} + \frac{1}{2}\right)^{P_z} \left(\frac{x}{L} + \frac{1}{2}\right)^{P_x} \tag{1}$$

$$V_{f1}(x,z) + V_{f2}(x,z) = 1 (2)$$

Within this framework, the gradient indices P_x and P_z denote the volume fraction's behavior along the entire length and thickness of the beam, respectively. Fig. 2 shows the variation of the volume fraction (V_{f1}) through a non-dimensional axial coordinate (x/L) along the length (L) of the beam and a non-dimensional transverse coordinate (z/h) across the thickness of the beam. The functional properties of material P(x,z) consisting of uniformly distributed 2DFGPCB can be represented by Eq. (3) [15].

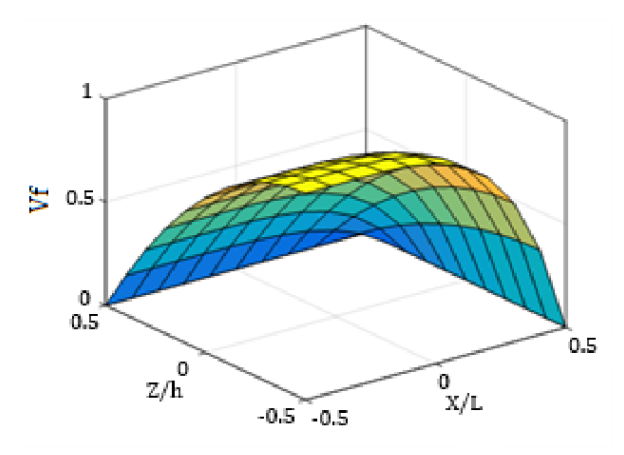


Fig. 2. Metal volume fractions in the direction of the nondimensional axial coordinate and the non-dimensional transverse coordinate

$$P(x,z) = (P_c - P_m) \left(\frac{z}{h} + \frac{1}{2}\right)^{P_z} \left(\frac{x}{L} + \frac{1}{2}\right)^{P_x} + P_m - \frac{\alpha}{2} (P_c + P_m)$$
 (3)

The symbol ' α ' represents the porosity index, which is a value between 0 and 0.3. The variable 'm' indicates the presence of metal, while 'c' indicates the presence of ceramic. Modulus of elasticity (E) is used to evaluate material rigidity and moment of inertia in an evenly distributed 2DFGPCB, and it may be mathematically represented as shown in Eq. (4) [16].

$$E(x,z) = (E_c - E_m) \left(\frac{x}{L} + \frac{1}{2}\right)^{P_x} \left(\frac{z}{h} + \frac{1}{2}\right)^{P_z} + E_m - \frac{\alpha}{L} (E_c + E_m)$$
 (4)

There is a little difference when utilizing Poisson's ratio compared to other attributes, which is considered unaffected because computations are performed using the mean value. Similarly, Eq. (5) [17] can be used to derive the impact characteristics of a distributed but even 2DFGPCB component.

$$P(x,z) = (P_c - P_m) \left(\frac{z}{h} + \frac{1}{2}\right)^{P_z} \left(\frac{x}{L} + \frac{1}{2}\right)^{P_x} + P_m - \frac{\alpha}{2} (P_c + P_m) \left(1 - \frac{2|z|}{h}\right)$$
 (5)

The modulus of elasticity for unevenly distributed 2DFGPCB can be approximated using Eq. (6) [18].

$$E(x,z) = (E_c - E_m) \left(\frac{z}{h} + \frac{1}{2}\right)^{P_z} \left(\frac{x}{L} + \frac{1}{2}\right)^{P_x} + E_m - \frac{\alpha}{2} (E_c + E_m) \left(1 - \frac{2|z|}{h}\right)$$
 (6)

FGP and FGB are crucial for static and dynamic structures, reducing manufacturing costs. Classic beam and plate theories often overestimate structural deflections, critical loads, and natural frequencies. Shear deformation and FGB theories enhance forecast precision. The 2DFGPCB Cartesian coordinate system, thickness, and porosity impact deformations and displacements. Constitutive equations determine the displacement field.

$$U(x,z) = \left(1 + \frac{z}{R}\right) u_0(x,t) - z \frac{\partial w_0}{\partial x}(x,t) + f(z) \left(\emptyset(x,t) + \frac{\partial w_0}{\partial x}(x,t)\right)$$
(7)

$$W(x,z) = w_0(x,t) \tag{8}$$

Axial displacement is represented by U(x,z), whereas transverse displacement is represented by W(x,z). At each certain location on the neutral axis, u_0 represents the axial displacement and w_0 represents the transverse displacement. The bending slope is represented by the partial derivative $(\partial w_0)/\partial x$, while \emptyset represents the shear slope. Use the shape function f(z) to figure out the transverse shear displacement, and Eqs. (7) and (8) can be used to find the mathematical equations that represent the non-zero stresses.

$$\varepsilon_{x} = \frac{\partial U}{\partial x} + \frac{W}{R} = (1 + \frac{z}{R}) \frac{\partial u_{0}}{\partial x} - z \frac{\partial^{2} w_{0}}{\partial x^{2}} + f(z) \left(\frac{\partial \phi}{\partial x} + \frac{\partial^{2} w_{0}}{\partial x^{2}}\right) + \frac{W_{0}}{R}$$
(9)

$$\varepsilon_z = \frac{\partial W}{\partial Z} = 0 \tag{10}$$

$$\gamma_{xz} = \frac{\partial U}{\partial z} + \frac{\partial w}{\partial x} - \frac{u_0}{R} \tag{11}$$

$$\gamma_{xz} = f'z \left[\emptyset + \frac{\partial w_0}{\partial x} \right] - \frac{u_0}{R}$$
 (12)

$$f(z) = z \left[\frac{1}{h} - \cos \frac{\pi}{3h} \right] \tag{13}$$

Through the utilization of Eqs. (9) and (11) in conjunction with Hooke's Law, the subsequent field equations can be formulated to represent stress:

$$\sigma_{x} = E(x)\varepsilon_{x} \tag{14}$$

$$\tau_{xz} = \frac{E(x)}{2(1+\mu)} \gamma_{xz} \tag{15}$$

2.2. Constitutive Equilibrium Equations

Hamilton's principle is a crucial topic in the field of bending analysis. The derivation of the essential equations of elasticity and dynamics is as described in reference [11].

$$B = \int_{t_1}^{t_2} (\delta U + \delta V) dt = 0$$
 (16)

 t_1 and t_2 represent time intervals. δU and δV represent variations in the potential energy of the strain, as well as the amount of work performed. The shift in strain energy that happens in a 2DFGPCB can be characterized.

$$\delta U = \frac{1}{2} \int_0^L \int_{-\frac{h}{2}}^{+\frac{h}{2}} (\sigma_x \varepsilon_x + \tau_{xz} \gamma_{xz}) dz dx \tag{17}$$

$$\delta V = -\int_0^L q \delta w_0 \, dx \tag{18}$$

Substituting equations. (9), (11), (14), and (15) into equation (16), strain energy could be deduced as,

$$B = \int_0^L \int_{-\frac{h}{2}}^{+\frac{h}{2}} (\sigma_x \varepsilon_x + \tau_{xz} \gamma_{xz}) dz dx - \int_0^L q \delta w_0 dx$$
(19)

$$= \int_{0}^{L} \int_{-\frac{h}{2}}^{+\frac{h}{2}} \left(\sigma_{x} \left(\frac{\partial u_{0}}{\partial x} - z \frac{\partial^{2} w_{0}}{\partial x^{2}} + f(z) \left(\frac{\partial \emptyset}{\partial x} + \frac{\partial^{2} w_{0}}{\partial x^{2}} \right) + \frac{w_{0}}{R} \right) + \tau_{xz} \left(f'z \left[\emptyset + \frac{\partial w_{0}}{\partial x} \right] - \frac{u_{0}}{R} \right) \right) dz dx - \int_{0}^{L} q \delta w_{0} dx$$
(20)

$$= \int_{0}^{L} \int \left(\left(N_{x} \frac{\partial u_{0}}{\partial x} - M_{x}^{b} \frac{\partial^{2} w_{0}}{\partial x^{2}} + M_{x}^{s} \left(\frac{\partial \emptyset}{\partial x} + \frac{\partial^{2} w_{0}}{\partial x^{2}} \right) + \frac{w_{0}}{R} \right) + \left(Q_{x} \left[\emptyset + \frac{\partial w_{0}}{\partial x} \right] - \frac{u_{0}}{R} \right) \right) dz dx - \int_{0}^{L} q \, \delta w_{0} \, dx$$

$$(21)$$

where M_x and Q_x values for shear force and bending moment, respectively. P_x and R_x represent the resultants of higher-order stresses.

$$N_{x} = \int_{-\frac{h}{2}}^{+\frac{h}{2}} \sigma_{x} dZ \tag{22}$$

$$M_{\chi}^{b} = \int_{-\frac{h}{2}}^{+\frac{h}{2}} \sigma_{\chi} z dZ \tag{23}$$

$$M_x^s = \int_{-\frac{h}{2}}^{+\frac{h}{2}} \sigma_x f(z) dZ \tag{24}$$

$$Q_{x} = \int_{-\frac{h}{2}}^{+\frac{h}{2}} \tau_{xz} f'(z) dZ$$
 (25)

2.3. Kuhn-Tucker Solution

The present study expands the use of KT conditions beyond traditional optimization to limited variational mechanics. The bending study of functionally graded porous beams with bi-directional grading and spatial porosity distributions reveals inhomogeneous stiffness and compliance properties. These variations inherently lead to inequality constraints, such as limits on deflections, stress concentrations, or local stiffness ratios that must remain physically permissible (e.g., non-tensile stress in metallic phases or porosity-induced compliance not surpassing structural thresholds).

The classical static beam formulation seeks to minimize the total potential energy functional, constituting an optimization issue. Nonetheless, the incorporation of porosity and gradient-index-dependent material inhomogeneity introduces limitations that conventional energy minimization fails to explicitly address. Consequently, KT criteria are used to represent these concealed inequality limitations, including:

- Ensuring positive definiteness of stiffness as porosity increases (i.e., modulus never becomes negative),
- Enforcing physical feasibility by preventing non-admissible deflection/stress states in graded porous regions,
- Capturing boundary-limited behaviors like non-slippage or support constraints when ceramic-rich zones meet boundary walls.

The optimization variables include the strain energy functional (via displacement fields u0, w0, ϕ), while the constraints pertain to gradient index limitations, porosity thresholds, and displacement compatibility at borders. The KT framework facilitates the integration of these physical constraints into the equilibrium formulation using Lagrange multipliers,

ensuring that all permissible requirements are met without the need for slack variables.

This aligns with recent research using KT-based variational formulations in FG structures for buckling Kannaiyan et al., [47] and vibration issues [48], whereby material heterogeneity and partial contact situations engender analogous constraint-driven behaviors. This research expands upon the existing framework to address the static deflection issue, showing its usefulness in modeling mechanically limited solutions inside multi-graded porous systems.

If the function $f_0(x)$ achieves a local minimum at point x^0 , subject to the set $K=x/(f_i(x)) \le 0$ (where i=1,2,3,...,m), and $f_k(x)$ (where k=0,1,2,...,m) are all differentiable, then there exists a vector of Lagrange multiplier U^0 that satisfies the following conditions [49].

$$\frac{\partial f_0(x^0)}{\partial x_j} + \sum_{i=1}^m U_i^0 \frac{\partial f_0(x^0)}{\partial x_j} = 0 \quad (j = 1, 2, 3, \dots, n)$$
(26)

$$f_i(x^0) \le 0 \ (i = 1, 2, 3, \dots, m)$$

$$u_i^0 f_i(x^0) = 0 \ (i = 1, 2, 3, ..., m)$$

$$u_i^0 \ge 0 \ (i = 1, 2, 3, \dots, m)$$

The conditions that are essential for a local minimum in optimization problems are referred to as the KT condition, while the non-negativity condition $U^0 \le 0$ is crucial for maximization problems, as presented in Fig. 3.

$$L(x, y, u) = f_0(x) + \sum_{i=1}^{m} u_i (f_i(x) + y_i^2)$$
 (27)

The necessary condition for its loca

$$\frac{\partial L}{\partial x_j} = \frac{\partial f_0(x^0)}{\partial x_j} + \sum_{i=1}^m u_i^0 \frac{\partial [f_i(x^0) + (y_i^0)^2]}{\partial x_j} = 0$$

(28)

$$\frac{\partial L}{\partial y_i} = 2u_i^0 y_i^0 = 0 \ (j = 1, 2, 3, n)$$
 (29)

$$\frac{\partial L}{\partial u_i} = f_i(x^0) + (y_i^0)^2 = 0 \quad (i = 1, 2, 3, \dots m) \quad (30)$$

$$\frac{\partial f_0[x^0(b)]}{\partial b_i} = -u_i^0 \ (i = 1, 2, 3, \dots m) \tag{31}$$

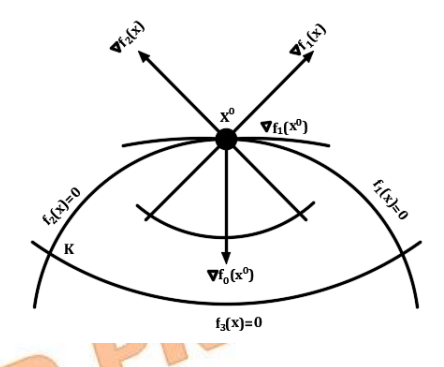


Fig. 3. Kuhn-Tucker condition [48]

Without slack variables, the mathematical problem,

$$L(x,u) = f_0(x) + \sum_{i=1}^{m} u_i f_i(x)$$
 (32)

The KT condition can be rewritten as [43],

$$\frac{\partial L(x^0, u^0)}{\partial x_j} = 0 \quad (j = 1, 2, 3, \dots, n)$$
 (33)

$$\frac{\partial L(x^0, u^0)}{\partial u_i} \le 0 \quad (i = 1, 2, 3, \dots, m) \tag{34}$$

$$u_i^0 \frac{\partial L(x^0, u^0)}{\partial u_i} = 0 \quad (i = 1, 2, 3, \dots, m)$$
 (35)

$$u_i^0 \ge 0 \ (i = 1, 2, 3, \dots m)$$
 (36)

When u_i is positive, it indicates that the corresponding i^{th} constraint is binding, indicating a boundary solution. The function $u_0(x, y)$, $w_0(x, y)$, and $U_0(x, y)$ can be mathematically represented as Lagrange equations when they are expressed as generalized coordinates. The KT condition, specified by the table values, can be expressed as follows.

$$u_0(x,y) = \sum_{i=1}^m f_i(x^0)\theta_i e^{i\lambda y}$$
(37)

$$w_0(x,y) = \sum_{i=1}^m f_i(x^0) \varphi_i e^{i\lambda y}$$
 (38)

$$\phi_0(x,y) = \sum_{i=1}^m f_i(x^0) \psi_i e^{i\lambda y}$$
(39)

where, θ_i , φ_i , and ψ_i are the three different boundary conditions and λ is the scalar. KT conditions are utilized for mathematical calculations as stated in Table 1.

$$\begin{bmatrix} S_{11}S_{12}S_{13} \\ S_{21}S_{22}S_{23} \\ S_{31}S_{32}S_{33} \end{bmatrix} \begin{bmatrix} u_0 \\ w_0 \\ \emptyset_0 \end{bmatrix} = \begin{bmatrix} 0 \\ q \\ 0 \end{bmatrix}$$
 (40)

$$S_{11}(i,j) = \frac{E(x,z)}{1-\mu^2} \int_0^L e^{\lambda x(x+1)} \,\theta_{i,x}, \theta_{j,x} dx \tag{41}$$

$$S_{12}(i,j) = \frac{E(x,z)}{1-\mu^2} \int_0^L e^{\lambda x(x+1)} \,\theta_{i,x}, \varphi_{j,x} dx \qquad (42)$$

$$S_{13}(i,j) = \frac{E(x,z)}{1-\mu^2} \int_0^L e^{\lambda(x+1)} \,\theta_{i,x}, \psi_{i,x} dx \tag{43}$$

$$S_{22}(i,j) = \frac{E(x,z)}{1-\mu^2} \int_0^L e^{\lambda x(x+1)} \varphi_{i,xx}, \varphi_{j,xx} dx$$
 (44)

$$S_{23}(i,j) = \frac{E(x,z)}{1-\mu^2} \int_0^L e^{\lambda x(x+1)} \, \varphi_{i,xx}, \psi_{j,xx} dx \quad (45)$$

$$S_{33}(i,j) = \frac{E(x,z)}{1-\mu^2} \int_0^L e^{\lambda x(x+1)} \psi_{i,xx} \psi_{j,xx} dx \qquad (46)$$

where, i, j = 1, 2, 3, n

3. Application-Result and Discussion

The numerical investigations based on USDT are carried out to predict the static analysis of FG porous beam with various conditions at the boundary like SS and CC as shown in Table 1.

Numerical findings are derived based on Navier's solutions. The FG porous beam consists of Aluminum metal with a modulus of elasticity (E_m) of 70 GPa, a Poisson's ratio (μ_m) of 0.3, and a density (ρ_m) of 2702 kg/m³. It also includes Alumina ceramic with a modulus (Ec) of 380 GPa, a Poisson's ratio (μc) of 0.3, and a density (ρ_c) of 3960 kg/m³. According to the powerlaw distribution, the properties of 2DFGPCB are changing in both the thickness and length directions.

Table 1. Boundary conditions based on the KT conditions solution method

15	Solution meti-	iou
Boundary Condition	x = 0	x = L
SS	u = 0, w = 0	w = 0
CC	u=0,w=0,	$u=0,w=0,\emptyset=0,$
	$\emptyset = 0, w' = 0$	w'=0
CS	$u = 0$, $\emptyset = 0$, $w = 0$,	u = 0, w = 0
	w' = 0	
CF	u=0, w=0,	
	$\emptyset = 0$,	

For the representation of results, the following dimensionless forms are used. Transverse displacement (w),

$$\overline{w} = \frac{w100E_m h^3}{q_0 L^4} \tag{47}$$

Table 2. Evaluation of dimensionless transverse deflection \overline{W} values of SS 2DFGPCB using different theories at different aspect ratios (L/h=5, L/h=20) and gradient index.

Method	Theory	$\epsilon_{\rm z}$	P=0	P=1	P=2	P=5	P=10
L/h=5, R/L= 5						- 6	F
[12]	Q3D	=0	3.1619	6.3264	8.1795	9.9816	11.0796
[12]	FSDT	=0	3.1437	6.2839	8.0803	9.6852	10.7148
Present	USDT	=0	3.1598	6.3163	8.1609	9.9786	11.0684
L/h=20, R/L= 5			DEV				
[12]	Q3D	=0	2.9672	5.9599	7.6597	9.1351	10.0549
[12]	FSDT	=0	2.9623	5.9507	7.6380	9.0648	9.9663
Present	USDT	=0	2.9664	5.9574	7.6579	9.1337	10.0478

Table 3. The dimensionless transverse deflection \overline{W} values of a SS 2DFGPCB with both even and uneven porosity, an aspect ratio of L/h=5, and gradient index are being considered.

Px&	L/h=5	Even porosi	ty		P _x &	L/h=5	Uneven poi	rosity	
P_z	0	0.1	0.2	0.3	Pz	0	0.1	0.2	0.3
0	3.1598	3.4131	3.7029	4.0464	0	3.1598	3.2297	3.2967	3.3667
1	7.38280	7.9595	8.6353	9.4364	1	7.3828	7.5318	7.6880	7.8513
2	10.0844	10.8721	11.7952	12.8894	2	10.0844	10.2879	10.5013	10.7243
5	13.6706	14.7384	15.9899	17.4732	5	13.6706	13.9465	14.2358	14.5381
10	16.0113	17.2620	18.7277	20.4650	10	16.0113	16.3344	16.6733	17.0273

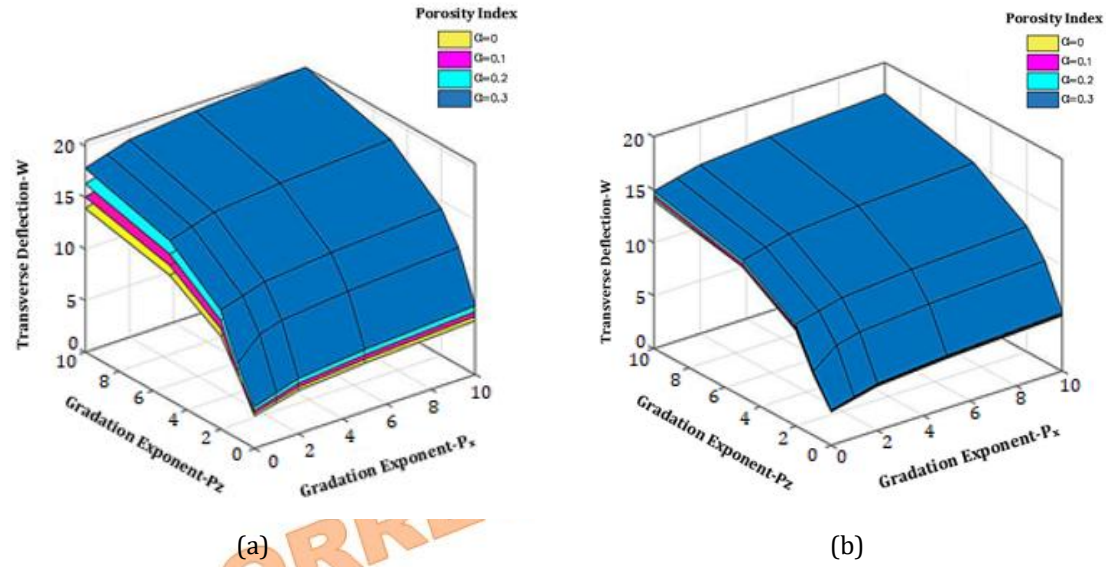


Fig.4. The dimensionless transverse deflection \overline{W} values of a SS 2DFGPCB with (a) even and (b) unequal porosity, at aspect ratio of L/h=5, and gradient index.

Table 4. Evaluation of dimensionless transverse deflection \overline{W} values of CC 2DFGPCB using different theories for different aspect ratios (L/h=5, L/h=20) and gradient index.

Method	Theory	$\epsilon_{\rm z}$	P=0	P=1	P=2	P=5	P=10
L/h=5, R/L= 5						RU	
[12]	Q3D	=0	0.4496	0.8591	1.1253	1.4788	1.6953
[12]	HOBT	=0	0.4437	0.8472	1.1090	1.4602	1.6761
Present	HSDT	=0	0.4458	0.8549	1.1162	1.4489	1.6901
L/h=20, R/L= 5	100	100					
[12]	Q3D	=0	0.2511	0.4834	0.6224	0.7736	0.8732
[12]	HOBT	=0	0.2527	0.4863	0.6263	0.7785	0.8787
Present	HSDT	=0	0.2496	0.4752	0.6119	0.7689	0.8701

Table 5. The dimensionless transverse deflection \overline{W} values of CC 2DFGPCB with both uniform and uneven porosity, an aspect ratio of L/h=5, and gradient index are considered.

P _x & P _z	L/h=5	Porosity ind	ex (Even dis	tribution)	P _x &	L/h=5 Por	osity index (1	Uneven dist	ribution)
	0	0.1	0.2	0.3	P_z	0	0.1	0.2	0.3
0	0.4458	0.5111	0.5876	0.6782	0	0.4458	0.4641	0.4836	0.5043
1	1.4982	1.6419	1.8145	2.0189	1	1.4946	1.5826	1.6266	1.6727
2	2.1644	2.3686	2.6077	2.8910	2	2.2211	2.2783	2.3393	2.4040
5	3.1418	3.4224	3.7511	4.1404	5	3.1985	3.2771	3.3609	3.4499
10	3.5831	3.8982	4.2674	4.7046	10	3.6398	3.7281	3.8222	3.9221

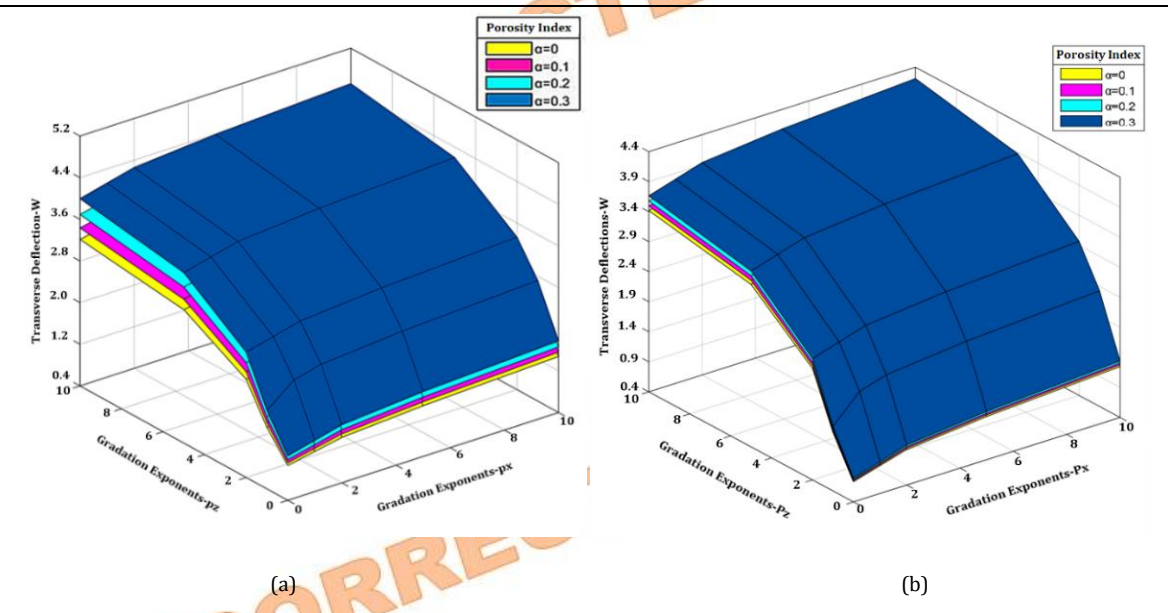


Fig. 5. The dimensionless transverse deflections w values of CC 2DFGPCB with both (a) even and (b) uneven porosity, an aspect ratio of L/h=5, and gradient index

Table 6. Evaluation of dimensionless transverse deflection \overline{w} values of CS 2DFGPCB using different theories for different aspect ratios (L/h=5, L/h=20) and gradient index.

			(, , ,	, 0			
Method	Theory	$\epsilon_{\rm z}$	P=0	P=1	P=2	P=5	P=10
L/h=5, R/L= 5						200	
[12]	Q3D	=0	0.7974	1.5573	2.0279	2.5811	2.9180
[12]	HOBT	=0	0.8057	1.5716	2.0469	2.6008	2.9376
Present	HSDT	=0	0.7913	1.5512	2.0236	2.5791	2.9119
L/h=20, R/L= 5	00	BI	17				
[12]	Q3D	=0	0.6365	1.2762	1.6381	1.9489	2.1444
[12]	HOBT	=0	0.6389	1.2810	1.6446	1.9567	2.1526
Present	HSDT	=0	0.6313	1.2707	1.6325	1.9436	2.1382

Table 7. Dimensionless transverse deflections \overline{w} values of CS 2DFGPCB with uneven and even porosity, aspect ratio (L/h=5), and gradient index.

P _x & P _z	L/h=5	Porosity inde	ex (Even dist	ribution)	Px & Pz	L/h=5 Porc	sity index (Uneven dist	ribution)
	0	0.1	0.2	0.3		0	0.1	0.2	0.3
0	0.7913	0.9046	1.0374	1.1948	0	0.7913	0.8635	0.9438	1.0335
1	2.5962	2.8509	3.1491	3.5024	1	2.5962	2.7587	2.9389	3.1403
2	3.7803	4.1276	4.5343	5.0161	2	3.7803	4.0019	4.2477	4.5224
5	5.3233	5.7913	6.3394	6.9887	5	5.3233	5.6221	5.9534	6.3235
10	6.1657	6.6997	7.3249	8.2656	10	6.1659	6.5066	6.8846	7.3067

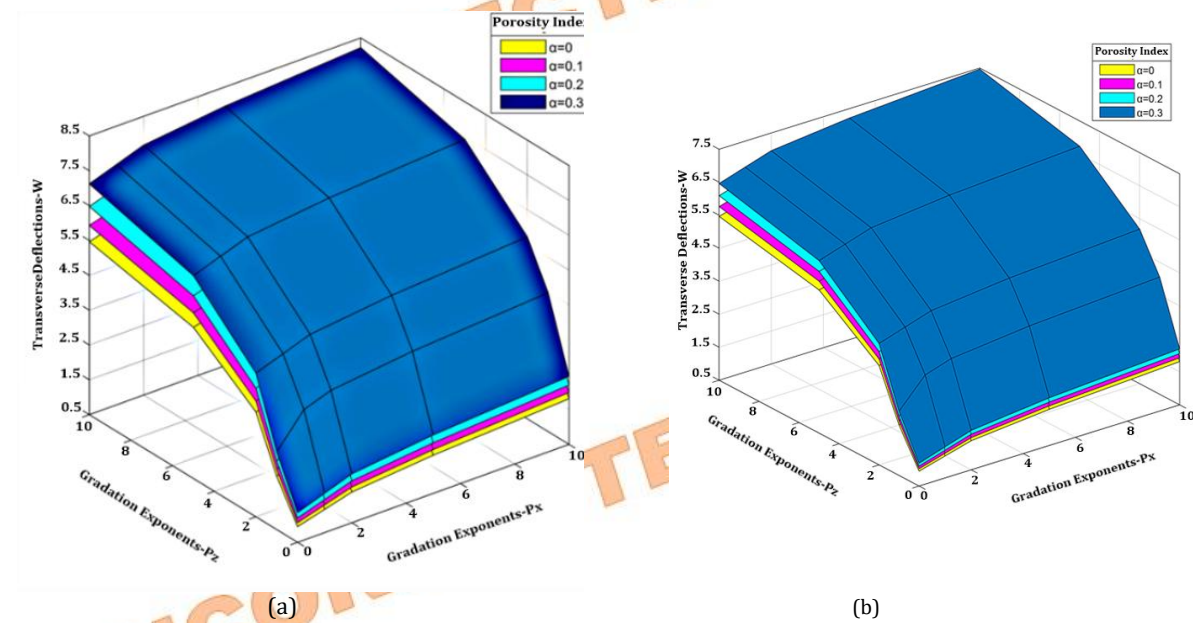


Fig. 6. Dimensionless Transverse deflections \overline{w} values of CS 2DFGPCB with (a) even (b) uneven porosity, aspect ratio (L/h=5), and gradient index.

Table 8. Evaluation of dimensionless transverse deflection \overline{w} values of CF 2DFGPCB using different theories for different aspect ratios (L/h=5, L/h=20) and gradient index.

							The second second
Method	Theory	ϵ_{z}	P=0	P=1	P=2	P=5	P=10
L/h=5, R/L= 5					- 0	30	
[12]	Q3D	=0	5.6999	11.3650	14.6559	17.7827	19.7180
[12]	HOBT	=0	5.7439	11.4787	14.8198	17.9847	19.9221
Present	HSDT	=0	5.6873	11.3586	14.6472	17.7786	19.6982
L/h=20, R/L= 5	100	Ms.					
[12]	Q3D	=0	5.3760	10.7879	13.8567	16.4993	18.1554
[12]	НОВТ	=0	5.4083	10.8630	13.9586	16.6249	18.2859
Present	HSDT	=0	5.3683	10.7797	13.8481	16.4876	18.1489

Table 9. Dimensionless transverse deflections \overline{w} values of CF 2DFGPCB with uneven and even porosity, aspect ratio (L/h=5), and
gradient index.

P _x &	Porosity in	idex (Even dis	stribution)		P _x & P _z	Porosity index (Uneven distribution)			
1 2	0	0.1	0.2	0.3	_ • z	0	0.1	0.2	0.3
0	5.6873	7.8109	10.2951	13.2402	0	5.6873	6.3269	7.0421	7.7717
1	36.7957	41.3538	46.6860	53.0076	1	36.7957	38.1684	39.6326	41.1987
2	60.0257	66.4018	73.8622	82.7037	2	60.0257	61.9460	63.9940	66.1849
5	81.9994	90.0952	99.5658	110.7938	5	81.9994	84.4022	87.0387	89.8204
10	97.8456	107.1816	118.1029	131.0508	10	97.8456	100.6573	103.6562	106.8640

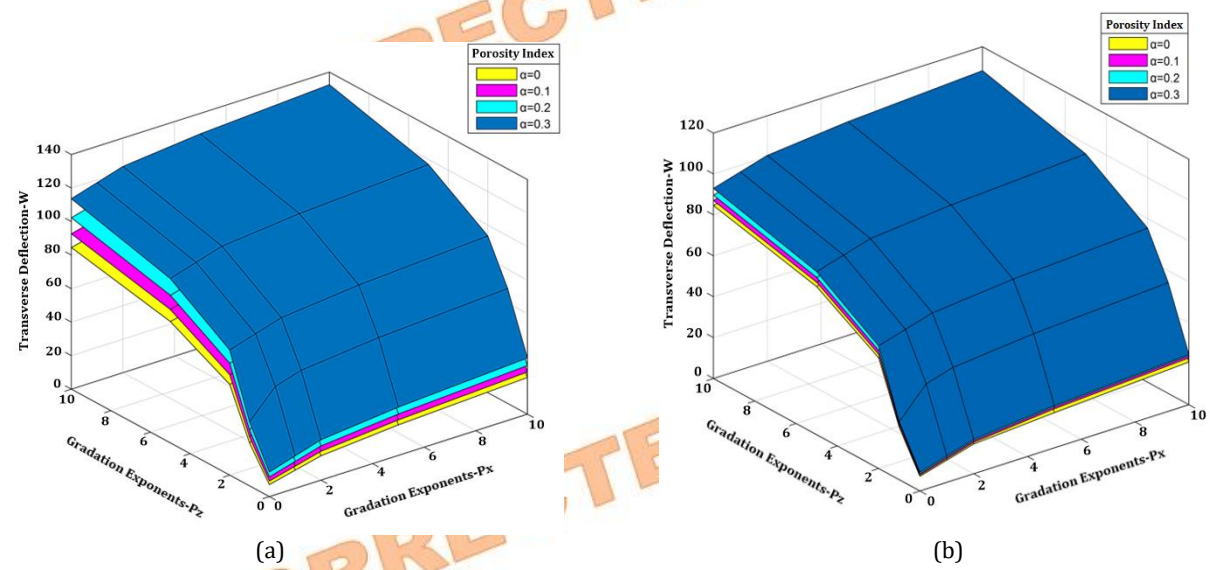


Fig. 7. Dimensionless Transverse deflections \overline{w} values of CF 2DFGPCB porous beam with (a) even (b) uneven porosity, aspect ratio (L/h=5), and gradient index.

4. Discussion

Analyzed 2-directional 2DFGPCB with porous material under UDL at various conditions at the boundary (SS, CC, CS, and CF), aspect ratios (L/h=5 & 20), and gradient index $(P_x = P_z=0, 1, 2,$ 5, and 10) and porosity index (α = 0, 0.1, 0.2, and 0.3) for finding dimensionless transverse deflections. Numerical values of transverse deflection are shown in Tables 2, 4, 6, and 8. The modulus of elasticity of a beam decreases as the value of its gradient index increases; hence, the transverse deflection increases as the gradient index increases in the x and z directions. In other words, its dimensionless transverse deflection values increase as the value of the power law exponent increases. Because a change in the conditions of the boundary indicates a change in the stiffness of the beam, the values of the nondimensional maximum deflection for the CF FGM beam are larger than those for the remaining boundary conditions (SS, CC, and CS) [36].

Tables 2, 4, 6, and 8 show the decrease in dimensionless transverse deflections, which is explained by the influence of the length of the beam, i.e., aspect ratio increases, which means the length is increased, leading to a decrease in dimensionless transverse deflections. It shows that as beams are scaled down in size, their bending stiffness improves since there is less material to bend. Transverse deflection values as a function of porosity index are tabulated in Tables 3, 5, 7, and 9. Since the flexural rigidity of the FG beam decreases with increasing porosity, transverse deflection increases in all boundary conditions as the porosity index rises (Figs. 4, 5, 6, and 7) [25].

The transverse deflection values of SS beams with uniform porosity experience a substantial increase as the porosity index rises. At a gradient index of 0, the deflection increases from 3.1598 to 4.0464 as the porosity index increases from 0 to 0.3, resulting in a 28.07% increase. At higher gradient indices, the following percentages are observed: 27.83% for P_x & P_z = 1, 27.85% for P_x & P_z = 2, 27.85% for P_x & P_z = 10. Conversely, beams that have unequal porosity show a less significant rise in transverse deflection values as the porosity index increases

[35]. With a gradient index of 0, the deflection rises from 3.1598 to 3.3667, indicating a 6.55% growth as the porosity index climbs from 0 to 0.3. The percentage increases for additional gradient indices are as follows: 6.34% for P_x & P_z = 1, 6.35% for P_x & P_z = 2, 6.35% for P_x & P_z = 5, and 6.35% for P_x & P_z = 10.

The transverse deflection values of CC beams with uniform porosity exhibit a substantial increase as the porosity index rises. At a gradient index of 0, the deflection increases from 0.4458 to 0.6782 as the porosity index goes from 0 to 0.3, resulting in a 52.16% increase. Higher gradient indices exhibit similar patterns: 34.75% for $P_x \& P_z = 1$, 33.52% for $P_x \& P_z = 2$, 31.82% for $P_x \& P_z = 5$, and 31.32% for $P_x \& P_z =$ 10. Conversely, beams that have unequal porosity show a less significant rise in transverse deflection values as the porosity index increases [26]. At a gradient index of 0, the deflection increases from 0.4458 to 0.5043, indicating a 13.12% increment as the porosity index rises from 0 to 0.3. The percentage increases for various gradient indices are as follows: 11.92% for $P_x \& P_z = 1$, 8.23% for $P_x \& P_z$ = 2, 7.85% for $P_x \& P_z = 5$, and 7.75% for $P_x \& P_z$ = 10. The transverse deflection is much higher for uniform porosity than for uneven porosity across all gradient indices. When the porosity is uniform, the deflection increases by around 31-52%. However, when the porosity is uneven, the increase ranges from approximately 8-13% across the investigated gradient indices.

The transverse deflection values of CS beams with uniform porosity experience a substantial increase as the porosity index rises. At a gradient index of 0, the deflection increases from 0.7913 to 1.1948 as the porosity index goes from 0 to 0.3, resulting in a 51.00% increase. Higher gradient indices exhibit comparable trends: 32.58% for $P_x \& P_z = 1$, 32.79% for $P_x \& P_z = 2$, 31.27% for $P_x \& P_z = 5$, and 34.06% for $P_x \& P_z =$ 10. Conversely, beams that have unequal porosity show a less significant rise in transverse deflection values as the porosity index increases. With a gradient index of 0, the deflection increases from 0.7913 to 1.0335, indicating a 30.59% growth as the porosity index rises from 0 to 0.3. The percentage increases for various gradient indices are as follows: 20.94% for $P_x \& P_z = 1$, 19.64% for $P_x \&$ $P_z = 2, 18.82\%$ for $P_x \& P_z = 5$, and 18.47% for P_x & $P_z = 10$. The transverse deflection is much higher for uniform porosity than for uneven porosity across all gradient indices [37]. When the porosity is uniform, the deflection increases by around 31-51%. However, when the porosity is uneven, the increase in deflection ranges from approximately 18-31% across the investigated gradient indices.

The transverse deflection values of CF beams with uniform porosity experience a substantial increase as the porosity index rises. With a gradient index of 0, the deflection rises from 5.6873 to 13.2402 as the porosity index climbs from 0 to 0.3, resulting in a 132.78% increase. At gradient indices, following higher the percentages are observed: 44.11% for $P_x \& P_z =$ 1, 37.66% for $P_x \& P_z = 2$, 35.07% for $P_x \& P_z = 5$, and 33.84% for $P_x \& P_z = 10$. Conversely, beams that have unequal porosity show a less significant rise in transverse deflection values as the porosity index increases. At a gradient index of 0, the deflection increases from 5.6873 to 7.7717, indicating a 36.63% increase when the porosity index rises from 0 to 0.3. The percentage increases for various gradient indices are as follows: 11.97% for $P_x \& P_z = 1$, 10.27% for $P_x \& P_z = 2$, 9.53% for $P_x \& P_z = 5$, and 9.22% for P_x & P_z = 10. The transverse deflection for a uniform porosity distribution exhibits much greater percentage increases across all gradient indices compared to the non-uniform porosity distribution. When the porosity is uniform, the deflection increases by around 33-133%. However, when the porosity is uneven, the increase varies from approximately 9-37% across the investigated gradient indices.

5. Conclusions

2DFGPCB was analyzed for the behaviour of bending, subjected to various conditions at the boundary (SS, CC, CS, and CF). Considering these conditions at the boundary with different aspect ratios and gradient index in x and z directions. An analysis of bending was performed with both uniform and non-uniform porosity distributions using the USDT. Implementing the power law, the effective properties of 2DFGPCB were determined. Several numerical examples demonstrated the impact of boundary conditions, porosity distribution, aspect ratios, and the gradient index in bending analysis. Dimensionless bending was examined, and the computed results were compared to those from previous studies. Results from the calculations were found to correlate highly with those from the past. It was investigated how the bending of 2DFGPCB is affected by aspect ratios, gradient indexes, and boundary conditions. The following are the most important results pertaining to nonporous FGBs:

- Gradient indexes in x and z increase transverse deflection. Which is explained by material stiffness: increasing the gradient index decreases the beam modulus of elasticity.
- Mid-plane axial stress is zero, but these values are not zero at the FGM beam midplane for other values of the gradient index.

SS

Due to the modulus of elasticity variation through the beam thickness, the neutral plane moves toward the top of the FGM beam.

- Conditions at the boundary affect beam rigidity; the non-dimensional maximum deflection with CF 2DFGPCB is higher than with the other conditions at the boundary (SS, CC, and CS)
- By choosing appropriate gradient indices, the bending of 2DFGPCB may be regulated to match the design requirements.
- Transverse deflection increases in all BCs as the porosity index rises, and this effect is more pronounced at high porosity values (from 10% to 51% of the porosity rate across all boundary conditions) due to a decrease in the flexural rigidity of the FGB at high porosity rates.

The present study provides a flexible and expandable method for studying next-generation FG structures that find use in high-performance engineering applications. The research should focus on developing the formulation to include thermal and dynamic loading conditions. The model's applicability in aerospace and hightemperature structural systems would increase through the addition of temperature-dependent material properties and time-dependent creep effects. The model will be tested through finite element simulations and experimental verify predicted validation deflection to profiles and stress distributions and to evaluate its performance under realistic loading and support conditions.

Nomenclature

2DFGPCB	2 Directional Functionally Graded Porous curved beam
CC	Clamped-Clamped
CF FG FGB FGM FGMP	Clamped-Free Functionally Graded Functionally Graded Beam Functionally Graded Material Functionally Graded Material Plates Functionally Graded Material Beams
USDT	Unified Shear Deformation Theory
HOBT FGP SDT HSDT	Higher Order Beam Theory Functionally Graded Plate Shear Deformation Theory Higher Order Shear Deformation Theory

	1 5 11
2D	Two Dimensional
3D	Three Dimensional
С	Ceramic
Е	Modulus of elasticity [GPa]
f(z)	Shear shape function
h	Height [m]
K	Shear correction factor
L	Length [m]
m	Metal
M_b	Resultant bending moment
M_S	Resultant moment due to shear deformation
N_x	Axial resultant force
p	Gradient index
p _x	Gradient index in the length direction
P_{z}	Gradient index in the thickness direction
q	Transverse Load
Q_{xz}	Resultant shear forces
x, y, z	Different coordinates along the length, width, and thickness directions of the beam
∂w_0	Bending slope
φ̂	Shear slope.
$V_{\rm f}$	Volume fraction
μ	Poisson's ratio
ρ	Mass density [Kg/m³]
α	Porosity index
[Ski]	Stiffness matrix
δυ	Variation of Strain Energy
δV	Variation of work done

Simply Supported

References

- [1] Sayyad, R.A., Rathi, V.R., Kolase, P.K., 2019. Bending Analysis of Functionally Graded Beam Curved In Elevation Using Higher Order Theory. *International Research Journal of Engineering and Technology*, 6(8).
- [2] Lezgy-Nazargah M., 2020. A four-variable global–local shear deformation theory for the analysis of deep curved laminated composite beams. *ActaMech*, *231*(4), pp. 1403–1434.
- [3] Beg, M.S., Yasin, M.Y., 2021. Bending, free and forced vibration of functionally graded

- deep curved beams in thermal environment using an efficient layer wise theory. *Mech Mater.*
- [4] Sayyad, A.S., Avhad, P.V., 2022. A new higher order shear and normal deformation theory for the free vibration analysis of sandwich curved beams. *Compos Struct*.
- [5] Hadji, L., Bernard, F., Zouatnia, N., 2023. Bending and free vibration analysis of porous functionally-graded (PFG) beams resting on elastic foundations. *Fluid Dyn Mater Process*, 19, pp.1043–1054.
- [6] Avcar, M., Hadji, L., Akan, R., 2022. The influence of Winkler-Pasternak elastic foundations on the natural frequencies of imperfect functionally graded sandwich beams. *Geomech Eng.*, *31*(1), pp. 99–112.
- [7] Sayyad, A.S., Avhad, P.V., Hadji, L., 2022. On the static deformation and frequency analysis of functionally graded porous circular beams. *Forces Mech.*
- [8] Chami, G.M., Kahil, A., Hadji, L., 2022. Influence of porosity on the fundamental natural frequencies of FG sandwich beams. *Mater Today Proc. 53*, pp. 107–112.
- [9] Pham, Q.H., Tran, V.K., Nguyen, P.C., 2022. Hygro-thermal vibration of bidirectional functionally graded porous curved beams on variable elastic foundation using generalized finite element method. *Case Stud Therm Eng.*, 40.
- [10] Ahmadi, I., Sladek, J., Sladek, V., 2023. Size dependent free vibration analysis of 2D-functionally graded curved nanobeam by Meshless method. *Mech Adv Mater Struct.*, pp.1–22.
- [11] Belarbi, M.O., Houari, M.S.A., Hirane. H., Daikh, A.A., Bordas, S.P.A., 2022. On the finite element analysis of functionally graded sandwich curved beams via a new refined higher order shear deformation theory. *Compos Struct*.
- [12] Armagan Karamanli, Nuttawit Wattanasakulpong, M., Lezgy-Nazargah, Thuc, P. Vo., 2023. Bending, buckling and free vibration behaviours of 2D functionally graded curved beams. *Structures*, *55*, pp. 778–798.
- [13] Nabil Hebbar, ImèneHebbar, DjamelOuinas, Mohamed Bourada, 2020. Numerical modeling of bending, buckling, and vibration of functionally graded beams by using a higher-order shear deformation theory. *Fratturaed Integrità Strutturale*, 52, PP. 230-246.

- [14] Abderrahim Razouki, Lhoucine Boutahar, Khalid EL Bikri, 2020. The Exact Analytical Solution of The Bending Analysis of Thick Functionally Graded Beams with Higher Order Shear Deformation Theory Using Differential Transform Method. International Journal of Advanced Research in Engineering and Technology, 1(5), pp. 194-203.
- [15] Chandra Mohana Reddy, G., Nathi Venu Kumar., 2022. Bending Analysis of 2-D Functionally Graded Porous Beams Based on Novel High Order Theory. *Journal of Engineering Science and Technology Review*, 15 (5), pp. 189 203.
- [16] Bridjesh, P., Chandra Mohana Reddy, G., Geetha, N.K., Ravikiran, C.H., Nagaraju, S., 2023. On Numerical Bending Analysis of Functionally Graded Porous Beam – Effect of Porosity Adapting Higher Order Shear Deformation Theory. Journal of Computational Applied Mechanics, 54 (1), pp. 49-67.
- [17] Bridjesh, P., Chandra Mohana Reddy, G., Geetha, N.K., Ravikiran, C.H., Nagaraju, S., 2023. On Numerical Buckling Analysis of two directional Porous Functionally Graded Beam Using Higher Order Shear Deformation Theory. Academic Journal of Manufacturing Engineering, 21 (1), pp. 105-119.
- [18] Chandra Mohana Reddy, G., Ravi Kiran, C.H., Nagaraju, S., Bridjesh, P., 2023. On Numerical Analysis of Refined Higher Order Shear Deformation Theory for Frequency Responses of Two-Directional Functionally Graded Taper Beams. *Academic Journal of Manufacturing Engineering*, 22(2), pp. 109-120
- [19] Hu, H., Yu, T., Lich, L.V., Bui, T.Q., 2021. Dynamic and static isogeometric analysis for laminated Timoshenko curved microbeams. *Eng Anal Bound Elem, 128*, pp. 90–104.
- [20] Pei, Y.L, Li, L.X., 2019. Comment on the Navier's solution in A sinusoidal beam theory for functionally graded sandwich curved beams. *Composite Structures*.
- [21] Wang, X., Yuan, Z., Jin, C., 2019. 3D free vibration analysis of multi-directional FGM parallel epipeds using the quadrature element method. *Appl Math Model, 68*, pp. 383–404.
- [22] Semsi Coskun, Jinseok Kim, Houssam Toutanji, 2019. Bending, Free Vibration, and Buckling Analysis of Functionally Graded

- Porous Micro-Plates Using a General Third-Order Plate Theory. *J. Compos. Sci.*, 3.
- [23] Jinseok Kim, Krzysztof Kamil Zur, Reddy, J.N., 2018. Bending, free vibration, and buckling of modified couples stress-based functionally graded porous micro-plates. *Composite Structures*.
- [24] Saad, M., Hadji, L., 2022. Thermal buckling analysis of porous FGM plates. *Mater Today: Proc*, *53*, pp. 196–201.
- [25] Hadji, L., Fallah, A., Aghdam, M.M., 2022. Influence of the distribution pattern of porosity on the free vibration of functionally graded plates. *Struct Eng Mech.*, 82(2), pp. 151–61.
- [26] Madan, R., Bhowmick, S., Hadji, L., Tounsi, A., 2022. Limit elastic speed analysis of rotating porous annulus functionally graded disks. *Steel Compos Struct.* 52(3), pp. 375–88
- [27] Yang, H, Dong, C., Wu, Y., 2020. Post buckling analysis of multi-directional perforated FGM plates using NURBS-based IGA and FCM. *Appl Math Model*, *84*, pp. 466–500.
- [28] Thai, S., Nguyen, V.X., Lieu, Q.X., 2022.

 Bending and free vibration analyses of multidirectional functionally graded plates in thermal environment: a three-dimensional Isogeometric approach. *Compos Struct*ures.
- [29] Chami, G.M.B., Kahil, A., Hadji, L., Madan, R., Tounsi, A., 2023. Free vibration analysis of multidirectional porous functionally graded sandwich plates. *Steel Compos Struct.*, 46(2), pp. 263–77.
- [30] Hadji, L., Bernard, F., Madan, R., Alnujaie, A., Ghazwani, M.H., 2023. Bending and buckling of porous multidirectional functionality graded sandwich plate. *Struct Eng Mech.*, 85(2), pp. 233–246.
- [31] Sidda Reddy, B., Suresh Kumar, J., Eswara Reddy, C., Vijaya Kumar Reddy, K., 2014. Static Analysis of Functionally Graded Plates Using Higher-Order Shear Deformation Theory. International Journal of Applied Science and Engineering, 12 (1), PP. 23-41.
- [32] Sidda Reddy, B., Suresh Kumar, J., Eswara Reddy, C., Vijaya Kumar Reddy, K., 2014. Free Vibration Behaviour of Functionally Graded Plates Using Higher-Order Shear Deformation Theory, *Journal of Applied Science and Engineering*, 17 (3), pp. 231-241.

- [33] Sidda Reddy, B., Vijaya Kumar Reddy, K., 2019. Thermomechanical behaviour of Functionally Graded Plates with HSDT, *Journal of Computational and Applied Research in Mechanical Engineering*, 11(2). pp. 365-379.
- [34] Sidda Reddy, B., Vijaya Kumar Reddy, K., 2020. Flexural behavior of porous functionally graded plates using a novel higher order theory. *Journal of Computational Applied Mechanics*, 51(2), pp. 361-373.
- [35] Sidda Reddy, B., Vijaya Kumar Reddy, K., Chinna Ankanna, B., 2020. Free vibration behavior of bi-directional functionally graded plates with porosities using a refined first order shear deformation theory. *Journal of Computational Applied Mechanics*, 51(2), pp. 374-388.
- [36] Sidda Reddy, B., Vijaya Kumar Reddy, K., 2024. Analyzing the Buckling Behavior of In-plane Bidirectional Functionally Graded Porous Plates. *Journal of Computational Applied Mechanics*, 55(3), pp. 322-339.
- [37] Sidda Reddy, B., Vijaya Kumar Reddy, K., 2020. A refined inverse hyperbolic shear deformation theory for bending analysis of functionally graded porous plates. *Journal of Computational Applied Mechanics*, 51(2), pp. 417-431.
- [38] Sayyad, A.S., Ghugal, Y.M., 2019. A sinusoidal beam theory for functionally graded sandwich curved beams. *Compos Struct*.
- [39] Karamanli, A., Vo, T.P., 2022. Finite element model for free vibration analysis of curved zigzag nanobeams. *Compos Struct.* 282.
- [40] Rezaiee-Pajand M, Masoodi AR. Stability analysis of frame having FG tapered beam-column. International Journal of Steel Structures. 2019; 19(2): 446-468.
- [41] Rezaiee-Pajand M, Rajabzadeh-Safaei N, Masoodi AR. An efficient mixed interpolated curved beam element for geometrically nonlinear analysis. Applied Mathematical Modelling. 2019; 76: 252-73.
- [42] Ghandehari MA, Masoodi AR, Panda SK. Thermal frequency analysis of double CNT-reinforced polymeric straight beam. Journal of Vibration Engineering & Technologies. 2024; 12(1): 649-65.
- [43] Mottaghi H, Masoodi AR, Gandomi AH. Multiscale analysis of carbon nanotubereinforced curved beams: A finite element approach coupled with multilayer

- perceptron neural network. Results in Engineering. 2024; 23: 102585.
- [44] Masoodi AR, Ghandehari MA, Tornabene F, Dimitri R. Natural frequency response of FG-CNT coupled curved beams in thermal conditions. Applied Sciences. 2024; 14(2):
- [45] Ghandehari, Moein A., Masoodi, Amir R., Hashemi, Sevved Mohammad Ali., Dynamic Characterization of Tapered Circular Curved Beams with Honeycomb-Shaped Sections Considering the Impact of Arbitrary Boundary Conditions. International Journal of Structural Stability and Dynamics. 2025.
- [46] Ghandehari MA, Masoodi AR. Employing GDQ method for exploring undamped vibrational performance of CNT-reinforced porous coupled curved beam. Advances in nano research. 2023; 15(6): 551-65.
- [47] Xiao Z. Generalized Karush-Kuhn-Tucker conditions in variational and set-valued analysis, Optimization and Control (math. OC) 1 (2020) 1-39.
- GN, Balasubramaniam [48] Kannaiyan Pappula B, Makgato S. Novel Kuhn-Tucker conditions for vibration analysis in a functionally graded porous beam using the R-program. Results in Engineering. 2024; 22:102064.
- [49] Kannaiyan GN, Balasubramaniam V. Novel Kuhn-Tucker conditions with R-program to analyze the buckling of a functionally graded porous beam. Journal of Mechanics of Materials and Structures.
- [50] Geetha N.K., Vivekanandam B., Bridjesh P.,



